DESIGN, CONTROL AND STABILITY ANALYSIS OF AN INTERLEAVED DC CONVERTER FOR VOLTAGE INTERFACING APPLICATION IN MICROGRIDS

Thiago Tricarico*, Matheus Soares*, Gustavo Gontijo*, Diego Oliveira*, Felipe Dicler*, Mauricio Aredes*

**Universidade Federal do Rio de Janeiro - UFRJ*
Rio de Janeiro, RJ, Brasil

Emails: thiago@lemt.ufrj.br, matheussoares@lemt.ufrj.br, gustavo@lemt.ufrj.br, diegosouza@lemt.ufrj.br, dicler@lemt.ufrj.br, aredes@lemt.ufrj.br

Abstract— This paper presents the modeling of an interleaved bidirectional dc-dc buck converter in order to design its average mode current control and the average mode voltage control. The converter is used as a voltage interface in a hybrid microgrid, which uses the dc link of a back-to-back converter as a connection point. Besides, a stability analysis is carried out. An analysis regarding the effect of the controllers bandwidth on the amplitude of the resonance observed in the closed-loop system is also presented. The cause of this resonance behavior is discussed based on the system model. The results have been obtained through the software PSCAD/EMTDC with the controller embedded in a DSP.

Keywords— Interleaved Converter, Hybrid Microgrid, Cascade Control, Stability Analysis.

Resumo— Este artigo apresenta a modelagem de um conversor cc-cc buck interleaved bidirecional para projetar seu controle de corrente e o controle de tensão. O conversor é usado como uma interface de tensão em uma micro-rede híbrida na qual o elo cc de um conversor back-to-back é utilizado como um ponto de conexão. Além disso, realiza-se uma análise de estabilidade. Por fim, apresenta-se uma análise referente ao efeito da largura de banda dos reguladores na amplitude de ressonância observada no sistema em malha fechada. A causa deste comportamento ressonante é discutida com base no modelo do sistema. Os resultados foram obtidos através do software PSCAD/EMTDC com os controladores embarcados em um DSP.

Palavras-chave— Conversor Interleaved, Micro-rede Híbrida, Controle em Cascata, Análise de Estabilidade.

1 Introduction

The ongoing trend of decentralized generation brings up new technical challenges to the operation of power systems, these challenges have led to the development of microgrids. When implemented in the ac form, these structures, can present problems regarding power quality and frequency regulation (Dragicevic et al., 2016).

Direct-current-based microgrids have been proposed in order to overcome the mentioned problems related to ac microgrids and to obtain a better integration with dc components such as photovoltaic generation, energy-storage systems and consumer's electronic devices. These components are deeply associated to the new distribution grids with the presence of distributed generation and with the development of the concepts of smart grids (Dragicevic et al., 2016).

In order to attain the advantages from both ac and dc microgrids while decreasing the need for multiple dc-ac conversions, some researchers have proposed the use of hybrid microgrids (Liu et al., 2011), one proposed method for implementing this kind of microgrid is to use the dc link of the back-to-back converter connecting the ac microgrid and the utility grid as the connection point for the dc microgrid (Majumder, 2014).

This configuration can add the necessity of a dc-dc converter to act as a voltage interface with bidirectional power flow capability. Interleaved converters, owing to their higher power density, modularity and higher reliability (Thounthong and Davat, 2010), present an attractive option to perform this voltage interface. However, this topology presents a serious drawback related to phase currents imbalance ((Schumacher et al., 2016); (Garcia et al., 2009) and (da Silva et al., 2016)). Some different techniques have been proposed aiming at overcoming this problem (Garcia et al., 2009).

The system topology studied in this work is depicted in figure 1. The back-to-back converter is responsible for controlling the ac voltage of the ac microgrid. The interleaved converter is used as an interface between the back-to-back dc-link and the dc microgrid bus. To the authors' best knowledge, this system configuration using a bidirectional interleaved converter has not been reported before.

The contribution of this work is an analysis of the controller bandwidth effect on the resonance frequency observed on the closed-loop system. The design of the controllers parameters is based on the methodology proposed in (Gao, 2003) with a modification on the integral gain of the voltage regulator. The influence of the control project on the stability margins is discussed. The system was modeled on PSCAD/EMTDC and the control law was embedded in a Texas Instruments DSP (Digital Signal Processor).

The remaining of this paper is organized as follows. In Section II and III, the design and the modeling of interleaved converter are presented, respectively. In Section IV, the linear control

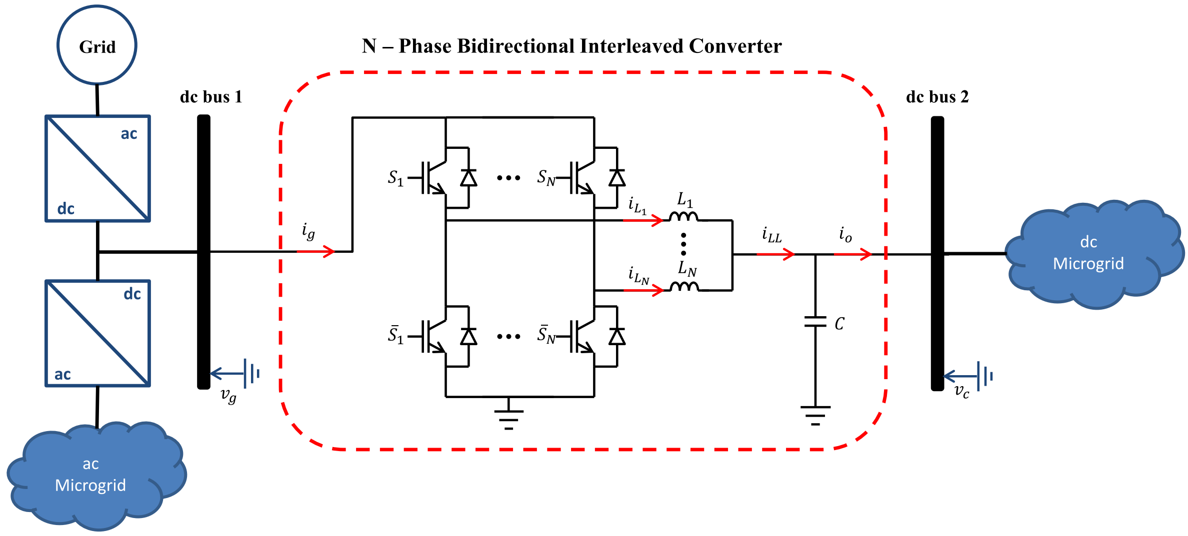

Figure 1: Hybrid microgrid system with a N-phase bidirectional interleaved converter as a power interface between the dc-link of the Back-to-Back converter (dc bus 1) and the dc microgrid bus (dc bus 2).

strategy and its project are discussed. In Section V, a stability analysis is carried out. Section VI presents the simulation results of the bidirectional interleaved converter operating as a power flow interface between an ac microgrid and a dc microgrid with two different dc links.

2 Interleaved Converter Design

The first Interleaved dc converter was proposed in 1971 for aerospace applications which demanded a high reliability converter (Garth et al., 1971). Its topology consists in the parallel connection of switching cells, leading to a converter containing parallel phases controlled by switching pulses with the same frequency, but phase shifted. Figure 1 shows the topology of a N-phase bidirectional interleaved converter performing a power flow interface between the dc link of the ac microgrid back-to-back converter and the dc bus of the dc microgrid.

This converter, amongst other advantages, allows for passive components of smaller size and leads to a low-ripple output current due to the shift of the current ripples in each phase of the converter (Miwa et al., 1992).

In (Chang, 1995), a method to determine the ripple reduction factor for a generic N-phase interleaved converter was proposed. Figure 2 shows the normalized current ripple as a function of the duty cycle.

The number of phases N can be chosen using the curves presented in figure 2, based on a desired reduction factor. One can note that as the value of N increases, greater ripple reductions are achieved in the output current (i_{LL}). The value of phase inductance can be designed based on the desired ripple in each phase (Δi_L), the switching frequency (f_{pwm}) and on the input and output dc voltage base values, as can be seen in (1).

$$L = \frac{V_{Cbase}}{f_{pwm}\Delta i_L}\left(1 - \frac{V_{Cbase}}{V_G}\right) \quad (1)$$

The output capacitance of the converter is the value of the dc bus capacitor, which is 3.3 mF in this work. The system electrical parameters are presented in table 1.

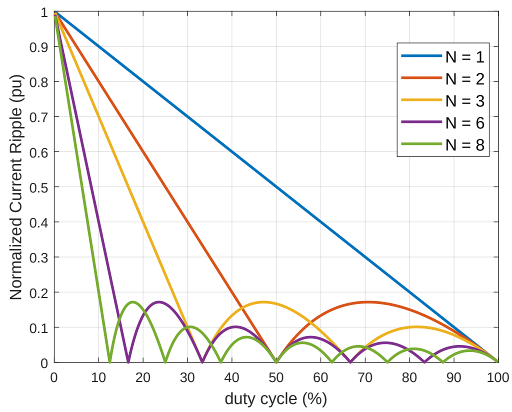

Figure 2: Normalized current ripple as function of the duty cycle and the number of phases N.

After designing the interleaved converter by determining the values of each phase inductance (L_k), the output capacitance (C) and the number of phases (N), it is necessary to determine a mathematical model in order to design the controller parameters.

Table 1: System Electrical Parameters

Microgrid Nominal Power (P_{base})	150 kW
Output Nominal Voltage (V_{base})	450 V
Nominal Current (I_{base})	333 A
Input Voltage (V_G)	980 V
Phase Resistance (R)	0.05 Ω
Phase Inductance (L)	2.0 mH
Output Capacitance (C)	3.3 mF
Number of Phases (N)	3
Switching Frequency (f_s)	5 kHz

3 Interleaved Converter Modeling

The generic N-phase interleaved converter equivalent circuit is depicted in figure 3. The variables $d_1 \ldots d_N$ represent the duty cycle of each phase. The dc microgrid system is represented as the current source (i_{Mcc}) in the equivalent circuit.

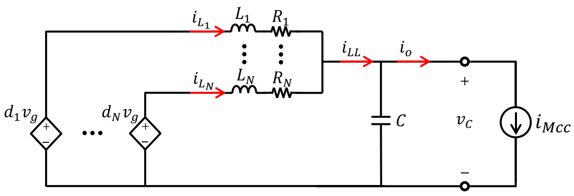

Figure 3: Bidirectional interleaved converter equivalent circuit for a generalized number of phases.

Using this circuit, the average large signal model is obtained from the Kirchhoff's laws, as shown in (2) and (3), where N is the total number of phases of the interleaved converter and $k = 1, \ldots, N$ represents a given phase k.

$$-d_k v_g + L_k \frac{di_{Lk}}{dt} + R_k i_{L_k} + v_c = 0 \quad (2)$$

$$\sum_{k=1}^{N} i_{L_k} - i_o - C\frac{dv_c}{dt} = 0 \quad (3)$$

Applying the Laplace Transform to (2) and (3) yields the frequency-domain model:

$$-d_k(s)V_g + (L_k s + R_k)I_{L_k}(s) + V_c(s) = 0 \quad (4)$$

$$\sum_{k=1}^{N} I_{L_k}(s) - I_o(s) - CsV_c(s) = 0 \quad (5)$$

In most applications, to avoid uneven current flow at each phase, the inductors employed in each of them are as similar as possible. Therefore, the approximations $L_1 = L_2 = \cdots = L_N = L$ and $R_1 = R_2 = \cdots = R_N = R$ will be considered valid. Using these approximations along with (4) yields:

$$-\sum_{k=1}^{N} d_k(s)\,V_g + (Ls+R)\sum_{k=1}^{N} I_{L_k}(s) + N\,V_c(s) = 0 \quad (6)$$

$$\sum_{k=1}^{N} I_{L_k} = \frac{\sum_{k=1}^{N} d_k(s)\,V_g - NV_c(s)}{(Ls+R)} \quad (7)$$

substituting the relation given by (7) into (5) yields:

$$\frac{\sum_{k=1}^{N} d_k(s)\,V_g - N\,V_c(s)}{(Ls+R)} - I_o(s) - CsV_c(s) = 0 \quad (8)$$

Through algebraic manipulations, the following equation is obtained:

$$\sum_{k=1}^{N} d_k(s)\,V_g - (Ls+R)\,I_o\,(s) - (LCs^2 + RCs + N)\,V_c(s) = 0 \quad (9)$$

Then, the relationship between each duty cycle $d_k(s)$, the load current i_o and the output voltage $V_c(s)$ is given by (10):

$$V_c(s) = \frac{V_g}{(LCs^2+RCs+N)}\sum_{k=1}^{N} d_k(s) - \frac{(Ls+R)}{(LCs^2+RCs+N)}\,I_o(s) \quad (10)$$

Further simplifying (10) results in:

$$V_c(s) = G_N(s)D_N(s) - Z_N(s)I_o(s) \quad (11)$$

where:
$G_N(s) = \dfrac{V_g}{(LCs^2+RCs+N)}$ is the no-load dc voltage gain between the input voltage V_g and the output voltage $V_c(s)$.

$D_N(s) = \sum_{k=1}^{N} d_k(s)$ is the modulation index of the N-phase interleaved converter and $Z_N(s) = \dfrac{(Ls+R)}{(LCs^2+RCs+N)}$ is the output impedance of the N-phase interleaved converter.

The open-loop transfer functions that describes the entire dynamics of the system can be also obtained through (4) and (5). In (12) it is observed the influence of the duty-cycles of each phase ($d_k(s)$) on the output voltage dynamics.

$$\frac{V_c(s)}{d_k(s)} = \frac{V_g}{LCs^2 + RCs + N} \quad (12)$$

The transfer function (13) rules the dynamics of the output voltage due to a load disturbance ($I_o(s)$).

$$\frac{V_c(s)}{I_o(s)} = -\frac{Ls+R}{sLCs^2 + RCs + N} \quad (13)$$

In (14) the effect of a given phase duty-cycle ($d_k(s)$) on its respective phase current ($I_{L_k}(s)$) is presented and (15) is the transfer function that describes the effect of the duty-cycles of a phase k ($d_k(s)$) on the current of another phase ($I_{L_n}(s)$).

$$\frac{I_{L_k}(s)}{d_k(s)} = \frac{V_g\left(CLs^2 + RCs + (N-1)\right)}{(CLs^2 + RCs + N)(Ls + R)} \tag{14}$$

$$\frac{I_{L_n}(s)}{d_k(s)} = \frac{V_g}{(CLs^2 + RCs + N)(Ls + R)} \tag{15}$$

The effect of the load current ($I_o(s)$) on the current phases ($I_{L_k}(s)$) and on the output current ($I_{LL}(s)$) are described in (16) and (17), respectively.

$$\frac{I_{L_k}(s)}{I_o(s)} = \frac{1}{CLs^2 + RCs + N} \tag{16}$$

$$\frac{I_{LL}(s)}{I_o(s)} = \frac{N}{CLs^2 + RCs + N} \tag{17}$$

The transfer function (18) presents the influence of the output current ($I_{LL}(s)$) on the output voltage ($V_C(s)$).

$$\frac{V_c(s)}{I_{LL}(s)} = \frac{1}{Cs} \tag{18}$$

This set of equations can describe any dynamics in the system states. The control project presented in this work focuses only on the dynamics of current and voltage, due to transfer functions (14) and (18), so as to design the controllers parameters.

4 Linear Control Project

The linear control strategy used in this work consists of a cascade control composed of an inner current loop for each phase and an outer voltage loop, as shown in figure 4. This strategy is used in order to ensure that current imbalance between the converter phases will not occur. The controller parameters are set based on the methodology proposed in (Gao, 2003), which ensures the desired bandwidths for the closed-loop transfer functions. A modification on the voltage regulator integral gain (K_{iv}) is proposed in order to achieve a better response when the system is under load variation.

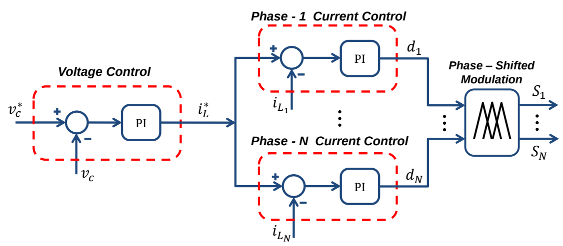

Figure 4: N-phase interleaved cascade control scheme and modulation.

As a matter of fact, this methodology, proposed originally in (Gao, 2003), which is valid for any generic control problem, has never been applied on the control of interleaved converters in the previous literature.

Figure 5 shows the feedback control system used in this work based on the modeling presented in the previous section. This system consists in both current and voltage PI regulators and the transfer functions presented in (14) and (18).

It is important to notice that the control project is performed in the per-unit system. Then, the electrical quantities are referred to their respective bases (V_{base}, I_{base} and P_{base})

4.1 *Current Control Project*

The current control is based on a PI controller that provides the duty cycle (d_k) for each phase. The design of the regulator parameters (K_{pc} and K_{ic}) is made by approximating the transfer function (14) by (19).

This approximation is valid since the poles and zeros of the transfer function (14), given by the roots of $LCs^2 + RCs + (N-1)$ and $LCs^2 + RCs + N$, respectively, are close enough to each other, so that they do not affect the system bandwidth.

$$G(s) = \frac{V_g}{Ls + R} \tag{19}$$

Hence, the controller parameters of the current closed-loop control system depicted in figure 6 can be determined based on the values of L, R, V_g, the current base (I_{base}) and the desired closed-loop bandwidth ω_c, as shown in (20) and (21).

$$K_{pc} = \frac{\omega_c\, L\, I_{base}}{V_G} \tag{20}$$

$$K_{ic} = \frac{\omega_c\, R\, I_{base}}{V_G} \tag{21}$$

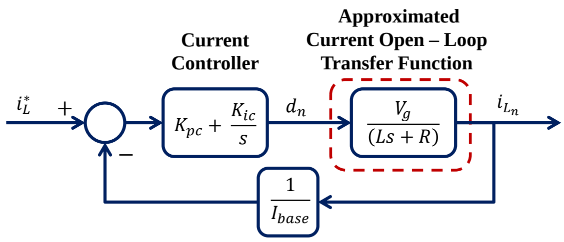

Figure 6: Current control loop.

4.2 *Voltage Control Project*

A similar approximation is made for the voltage loop so as to design the values of K_{pv} and K_{iv}. The current closed-loop control system has a behavior similar to a low pass filter with bandwidth ω_c, as can be seen in figure 7.

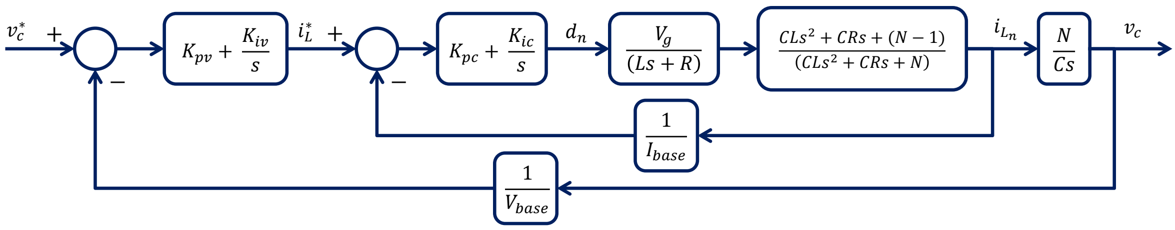

Figure 5: N-phase interleaved feedback control system diagram.

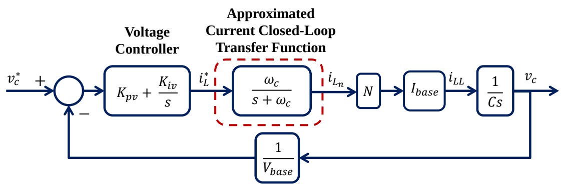

Figure 7: Voltage control loop.

It is well known that in a cascade controller the inner regulator bandwidth must be larger than the outer regulator bandwidth ($\omega_c > \omega_v$). In this case, the dynamics of current control can be disregarded and the voltage controller proportional gain (K_{pv}) can be set as follows:

$$K_{pv} = \omega_v \frac{C}{N} \frac{V_{base}}{I_{base}} \tag{22}$$

In an ideal converter, only a proportional gain (K_{pv}) would be necessary to regulate the output voltage with zero steady-state error and to guarantee the desired closed-loop bandwidth ω_v. However, in real converters the losses in the dc link cause a steady-state error in the output voltage.

Due to this fact, it is necessary to use an integrator in order to ensure the desired operational voltage. Besides, the regulator must have the ability to reject the output voltage disturbance related to the load current (I_o). This work proposes the use of an integral gain (K_{iv}) shown in (23).

$$K_{iv} = \frac{\gamma \omega_v C}{N} \frac{V_{base}}{I_{base}} \tag{23}$$

Where γ is a gain that can be set so as to make the system operate with a fast load disturbance rejection response. The next section will show the influence of the previously mentioned control parameters ($\omega_c, \omega_v, \gamma$) on the closed-loop performance.

5 Stability Analysis

In the previous section, a voltage regulator integral gain (K_{iv}) was introduced, which is a function of the parameter γ and can be set as a function of the current closed-loop bandwidth (ω_c) so as to improve the time response of the system when submitted to load variation.

Figure 8 shows the output voltage sag, caused by a load step, for different values of γ. One can note that, as the value of γ increases, the time response is improved. However, for values above a certain limit, voltage overshoot is observed.

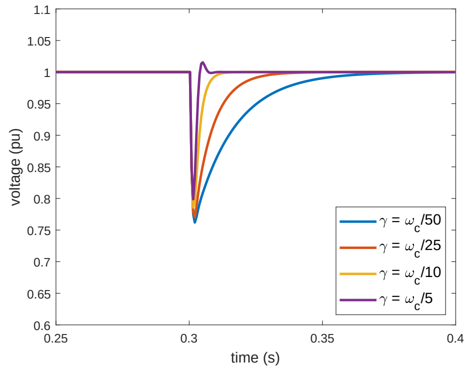

Figure 8: Effect of γ on the output load disturbance rejection ($\omega_c = 1000\pi \; rad/s$, $\omega_v = 400\pi \; rad/s$).

In figure 9, the Bode diagram of the current closed-loop transfer function is depicted, it can be stated that the resonance observed at the frequency ω_{rc} is due to the complex closed-loop poles related to those open-loop poles and zeros neglected in the previous section. The bandwidth of the current closed-loop transfer function is consistent with the desired value ω_c, though.

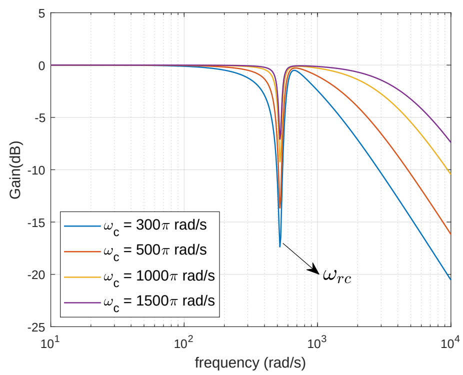

Figure 9: Bode diagram of the current control closed-loop transfer function.

The presence of these poles can be observed on the root locus of the current control system, shown in figure 10(a).

The current overshoot reduction is observed when higher values of ω_c are used as can be seen in figure 10(b) and can be confirmed analyzing the corresponding resonance peaks in figure 9. It is possible to observe that for bandwidth values greater than $1300\pi\ rad/s$ the system step response indicates a current overshoot smaller than 5%.

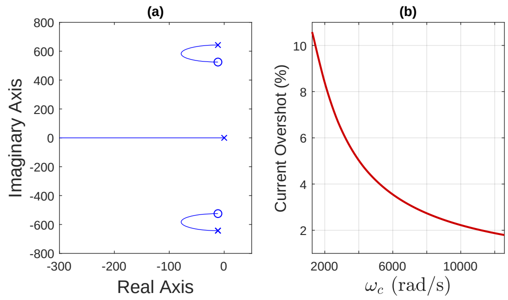

Figure 10: (a) Root locus of the current control loop and (b) current overshoot in function of ω_c.

Figure 11 shows the closed-loop voltage control Bode diagram for different values of bandwidth ω_v. In this case, the current controller has a bandwidth equal to $\omega_c = 1000\pi\ rad/s$.

One can notice that the higher the value of ω_v, the smaller the resonance amplitude in the frequency ω_{rv} although, other resonance frequencies different than ω_{rv} start to appear.

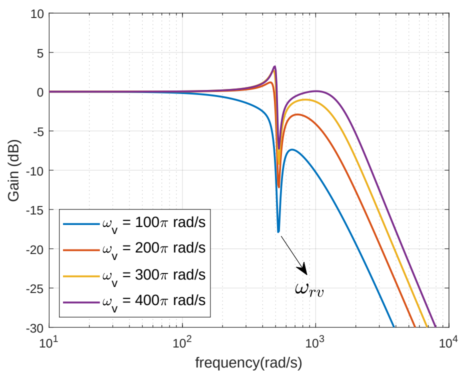

Figure 11: Bode diagram of the voltage control loop.

As mentioned in the previous section, the voltage control design is made based on two approximations. The first one is to disregard the effects of the complex poles in the current loop. The second is to consider the closed-loop current control transfer function as a low-pass filter with unit gain and bandwidth at ω_c.

Figure 12 shows the voltage controller step response for both cases when the poles and zeros are considered and when they are neglected, leading to the approximated transfer function.

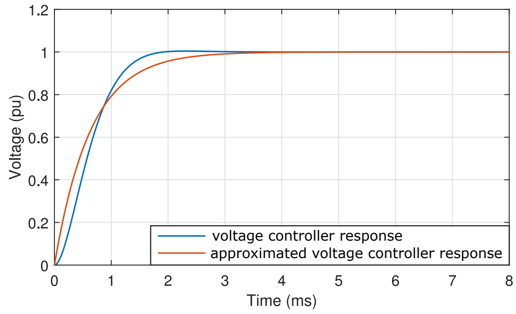

Figure 12: Unit-step response of the voltage controller when the poles and zeros are taken into account and when they are neglected.

The open-loop frequency response of both current loop and voltage loop are depicted in figure 13.

It can be observed in (a) that the current regulator parameters, designed according to (20) and (21), leads to a phase margin of 90°, which guarantees a smooth response. The voltage loop has a phase margin of (58°) as can be seen in (b).

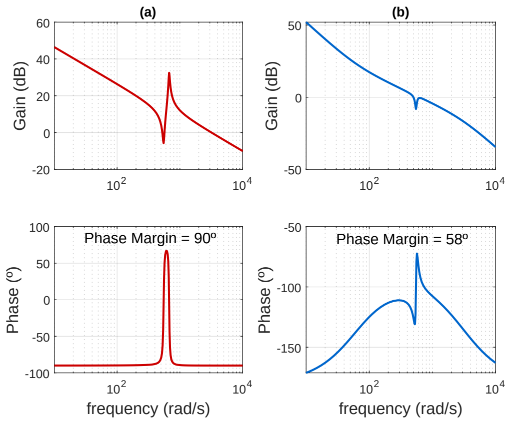

Figure 13: (a) Open-loop frequency responses of the current control system and (b) the voltage control system - ($\omega_c = 1000\pi\ rad/s$, $\omega_v = 400\pi\ rad/s$, $\gamma = 20\pi$).

6 Simulation Results

The simulation of the system presented in figure 1 was carried out on the software PSCAD/EMTDC in a Processor-in-the-Loop (PIL) configuration in which the control source code is embedded on a Texas Instruments DSP (TMS320F28377S) and the interchange of signals between both of them is made through a serial communication protocol.

The simulation of the system presented in figure 1 was carried out on the software PSCAD/EMTDC in a Processor-in-the-Loop (PIL) configuration in which the control source code is embedded on a Texas Instruments

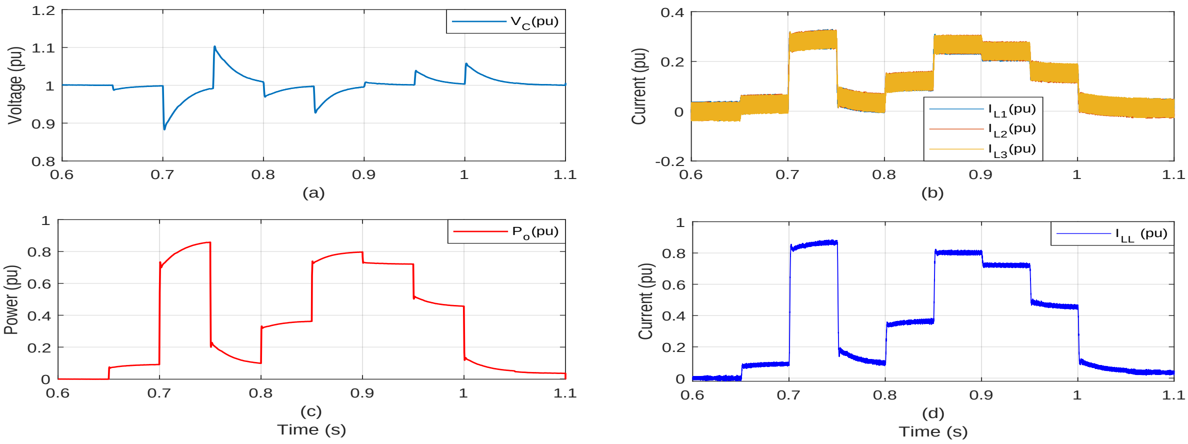

Figure 14: Interleaved converter's output voltage (a), phase currents (b), power flow (c) and output current (d) when operating under a random power profile - ($\omega_c = 1000\pi rad/s, \omega_v = 400\pi rad/s, \gamma = 20\pi$).

DSP (TMS320F28377S) and the interchange of signals between both of them is made through a serial communication protocol.

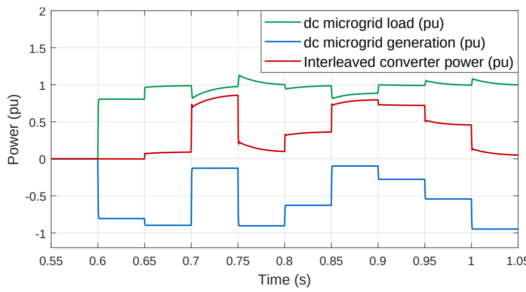

Figure 15: Load and generation profile of the dc microgrid.

In the worst case scenario, when a total power flow inversion (from $-1.0\,pu$ to $1.0\,pu$) happens, the voltage sag reaches a value of $0.7\,pu$, as shown in figure 16.

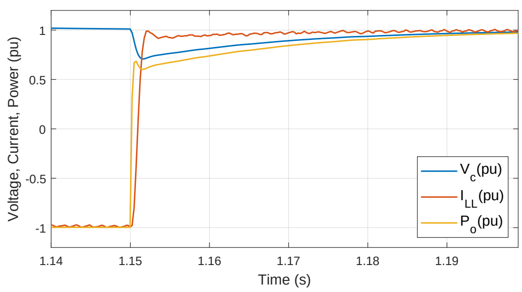

Figure 16: Dynamics of the output voltage when subjected to a power flow inversion.

It is observed that both output current (i_{LL}) and converter's power (P_o) have no overshoot since the voltage controller gives a dampened reference to the current controllers, which have a phase margin of 90^o that ensures a smooth response.

Figure 17 shows the phase currents with shifted ripples (a) and the output current, with low ripple (b). It can be noted that the output current (i_{LL}) has a reduction in its ripple to a value below 2%. None current imbalance is observed on the operation of the interleaved converter since the current controllers of each phase ensure their current regulation.

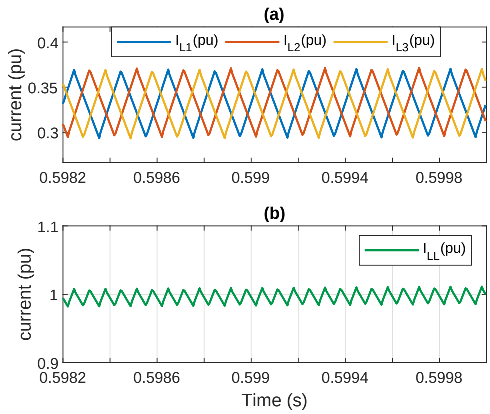

Figure 17: (a) Current ripples in each of the three phases of the interleaved converter; (b) Output current ripple.

In figure 18, the power profile of the entire hybrid microgrid is presented. In this scenario, it is shown in (a) the ac and dc microgrids power profile and in (b) the active power injected to the utility grid. As a matter of fact, the power delivered by the dc microgrid through the interleaved converter feeds the ac microgrid loads and the amount of excessive power, generated by the power sources at the dc microgrid, is injected into the ac utility grid through the back-to back converter. In (c), the dc microgrid voltage dynamics under the previously mentioned scenario can be observed.

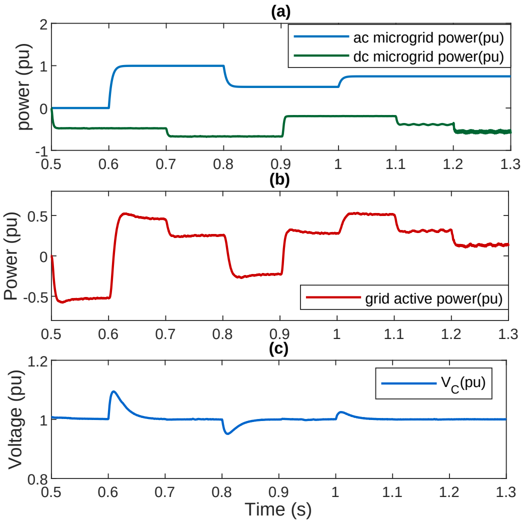

Figure 18: (a) ac and dc microgrids power profile, (b) active power inject into the grid and (c) back-to-back dc link voltage.

7 Conclusion

In this work, an accurate modeling of the N-phase bidirectional interleaved converter is developed in order to design its cascade control. The effects of the voltage vibration modes in the current closed-loop control system response and its reduction by setting the controllers bandwidths properly were demonstrated. A modification of the voltage regulator integral gain in order to improve the system transient response was introduced. Simulation results have shown a stable operation of the interleaved converter performing a voltage interface between an ac microgrid and a dc microgrid for different kinds of load and generation profiles in the dc microgrid. This stable behavior is achieved due to the proposed control parameters design, which ensures a high phase margin for both current and voltage control-loops. As future works, it can be highlighted that it is necessary to study the load current effects on the output voltage dynamics. Besides, a stability study concerning the effects of input voltage disturbances should be done.

Acknowledgments

The authors acknowledge the financial support from FAPERJ.

References

Chang, C. (1995). Current ripple bounds in interleaved DC-DC power converters, *Proceedings of 1995 International Conference Power Electronics and Drive Systems PEDS 95*, pp. 738–743.

da Silva, J. L., dos Reis, G. L., Seleme Jr, S. I. and Meynard, T. (2016). Control Design and Frequency Analysis of an Output Filter in Parallel Interleaved Converters, *2016 IEEE International Conference on Power and Energy (PECon)*, pp. 734–739.

Dragicevic, T., Lu, X., Vasquez, J. C. and Guerrero, J. M. (2016). Dc microgrids part i: A review of control strategies and stabilization techniques, *IEEE Transactions on Power Electronics* **31**: 4876 – 4891.

Gao, Z. (2003). Scaling and bandwidth-parameterization based controller tuning, *Proceedings of the 2003 American Control Conference*, pp. 4989 – 4996.

Garcia, O., Zumel, P., de Castro, A., Alou, P. and Cobos, J. (2009). Current Self-balance Mechanism in Multiphase Buck Converter, *IEEE Transactions on Power Electronics* **24**: 1600–1606.

Garth, D. R., Muldoon, W. J., Benson, G. C. and Costague, E. (1971). Multi-phase, 2-kilowatt, high-voltage, regulated power supply, *1971 IEEE Power Electronics Specialists Conference*, pp. 110 – 116.

Liu, X., Wang, P. and Loh, P. C. (2011). A Hybrid AC/DC Microgrid and Its Coordination Control, *IEEE Transactions on Smart Grid* **2**: 278 – 286.

Majumder, R. (2014). A Hybrid Microgrid With DC Connection at Back to Back Converters, *IEEE Transactions on Smart Grid* **5**: 251 – 259.

Miwa, B. A., Otten, D. M. and Schlecht, M. F. (1992). High-efficiency power factor correction using interleaving techniques, *Proc. IEEE Applied Power Electronics Conference (APEC '92)"*, pp. 557–568.

Schumacher, D., Magne, P., Preindl, M., Bilgin, B. and Emadi, A. (2016). Closed loop control of a six phase interleaved bidirectional dc-dc boost converter for an EV/HEV application, *2016 IEEE Transportation Electrification Conference and Expo (ITEC)*, pp. 1–7.

Thounthong, P. and Davat, B. (2010). Study of a multiphase interleaved step-up converter for fuel cell high power applications, *Energy Conversion and Management* **51**: 826–832.